SHAPE-CONSISTENT GENERATIVE ADVERSARIAL NETWORKS FOR MULTI-MODAL MEDICAL SEGMENTATION MAPS

*Leo Segre** *Or Hirschorn** *Dvir Ginzburg* *Dan Raviv*

Tel Aviv University

ABSTRACT

Image translation across domains for unpaired datasets has gained interest and great improvement lately. In medical imaging, there are multiple imaging modalities, with very different characteristics. Our goal is to use cross-modality adaptation between CT and MRI whole cardiac scans for semantic segmentation. We present a segmentation network using synthesised cardiac volumes for extremely limited datasets. Our solution is based on a 3D cross-modality generative adversarial network to share information between modalities and generate synthesized data using unpaired datasets. Our network utilizes semantic segmentation to improve generator shape consistency, thus creating more realistic synthesised volumes to be used when re-training the segmentation network. We show that improved segmentation can be achieved on small datasets when using spatial augmentations to improve a generative adversarial network. These augmentations improve the generator capabilities, thus enhancing the performance of the Segmentor. Using only 16 CT and 16 MRI cardiovascular volumes, improved results are shown over other segmentation methods while using the suggested architecture. Our code is publicly available[1].

1. INTRODUCTION

Semantic segmentation is a key perceptual function in computer vision, aiming to densely categorize an image into meaningful distinguished areas. In the medical imaging domain, semantic segmentation is vital, providing tools for diagnostics, treatment planning, and prognosis. For disease diagnostics and surgical needs, multiple imaging modalities are available such as MRI, CT, and X-ray.

Traditional machine learning methods, such as atlas and model-based methods, showed good performance in cardiac image segmentation. However, they usually require features engineering which differs between image modalities [1]. In contrast, deep learning algorithms show promising results while implicitly discovering features from the data. They have been widely adopted for various tasks, from 2D binary segmentation [2] to multi-class 3D segmentation [3].
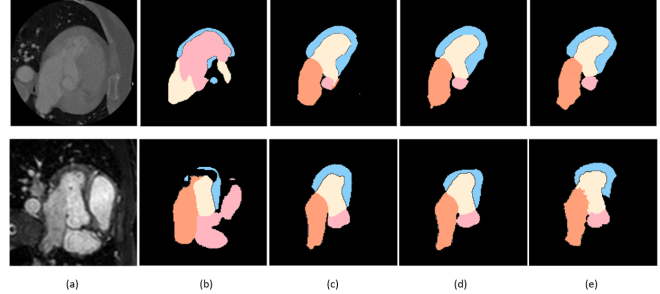

Fig. 1. Segmentation results generated by our method on cardiac CT images (top) and MRI (bottom). a) Examples of test images, b) Segmentation results without preprocess augmentations, c) Segmentation results without synthesized data, d) Segmentation results of our full method, e) The ground truth.

However, to achieve satisfying results, a sufficiently large number of training samples is required. As demonstrated in figure 1, the results of semantic segmentation when the training set is too small are significantly degraded. Segmented medical imaging datasets are hard to acquire and use due to strict regulations, lack of support from hospitals in acquiring the data, and high costs of medical imaging services. As medical images acquired using different modalities have very different characteristics, it is especially challenging to obtain data for new imaging modalities. This also applies to images from the same modality, captured using different scanning machines.

To overcome the lack of data, a common way to generate synthesized data is to use augmentations on the original data [4]. Another way to generate synthesized data is using a Generative Adversarial Network (GAN). This can be done directly by separate GAN for each domain, but it is even more effective to use cross-modality GAN and share information between modalities and generate more accurate synthesized data [5, 6]. Although some models used GANs as a proxy task to the segmentation objective on very small datasets [5], the mentioned method used 2D slices instead of 3D volumes thus discarding crucial information regarding the spatial consistency in the Z-axis. This paper presents a method to use deep learning based segmentation on a limited dataset by

using augmentations and generating 3D synthesized shape-consistent data. The presented method provides significant improvements in the limited training data domain, with an average accuracy increase of 15.9% in the final segmentation score. Additionally, we provide our code for future works.

2. RELATED WORK

Using deep learning for domain adaptation in a supervised or unsupervised manner has recently gained popularity [5, 7, 8, 9]. As the availability of training data from the same set of subjects in both source and target modalities is undesirable (requires multiple scans from each subject), an unsupervised cross-modal image synthesis, without pairing training data approach is beneficial [7].

Since the rise of deep learning, image to image translation is usually formulated as a pixel to pixel mapping using CNN's (Convolutional Neural Network) encoders and decoders [6, 10, 8]. CycleGAN had wide success, where bi-directional image translations are learned by two GANs separately, and the consistency constraint between transforms is enforced to preserve semantic information between transformed outputs [11]. The good results and robustness Cycle-GAN showed for many applications made it a popular backbone in future works. Thus, many unpaired image to image transformations are based on this framework with additional constraints to further regularize the transformation process. Although CycleGAN was initially proposed for 2D images, GANs have also been applied in 3D [12].

For medical image processing, adversarial learning has presented great efficiency on a variety of tasks [13]. Using synthetic data as augmented training data helps the segmentation network as seen for brain MRI and CT images [9]. *Zizhao Zhang et al.* [6] used a segmentation network to force shape consistency of the output transformed domain, using a private massive data set. As massive datasets are usually hard to acquire in this domain, our work avoids this demand, presenting great results using a public dataset with only 20 CT and 20 MRI samples. SIFA [5] used a novel approach of fusing feature and image appearance adaptation and applied it to cross-modality segmentation of cardiac volumes, but was limited to 2D slices, losing z-axis shape data.

3. METHODS

The method is applied in three phases. First, a segmentor is trained with the original data. Then, a 3D cycle and shape consistent GAN network is trained to create synthesized cardiac volumes, which is used later to train the segmentor in phase 3 and achieve the goal of improving the 3D segmentor network. Figure 2 illustrates the proposed architecture for domain adaptation in cardiac volumes.

3.1. Synthetic Data Generation

First, all scans aligned to RAS+ orientation and following *Cheng Chen et al.* [5] we manually cropped the MRI scans around the heart. To align between the CT scans and MRI scans, we also resized the CT scans into 256x256xZ, where Z preserves the original scan width-depth ratio. Then, using TorchIO [4] we randomly applied numerous 3D transformations on both the cardiac volumes and labels, specifically designed for medical data: normalization, random anisotropy - Simulates an image that has been acquired using anisotropic spacing and resampled back to its original spacing, random elastic deformation - A random displacement according to a grid of control points, random affine - applies affine transformation and resamples back to the original spacing. We observed the best results for 200 3D synthetic augmented scans, as more synthetic scans resulted in significantly longer run times and negligible improvements.

3.2. Volume to Volume Translation

For two unpaired domains A and B, we employ generative adversarial networks using a generator G and a discriminator D for each domain. The volume to volume translation is based on CycleGAN U-Net architecture enhanced to 3D volumes using 3D convolutions. The generator transforms the input domain A to the other domain B, the notation for this transformation is $G_B(X_A)$. The discriminator competes with the generator, trying to distinguish between a fake volume $G_B(X_A)$ and a real volume x_B. L2 loss is used to minimize the generator's objective of creating realistic volumes, noted as $\mathcal{L}_{adv,A}$.

We adopt the CycleGAN's approach of cycle consistency loss. Thus, we force the generators to reconstructed synthesized volumes $G_A(G_B(x_A))$ and x_A to be identical. We encourage the transformed volumes to preserve content from the original volume using L1 loss:

$$\mathcal{L}_{cycle,A} = -\frac{1}{N}\sum_i |x_A - G_A(G_B(x_A))|$$

Using the above constraints can lead to geometrically distorted transformations. The cycle consistency loss isn't enough to prevent spatial distortions. It is possible for generator B to create a distortion F and for generator A to apply the reverse transformation F^{-1} leading back to the original shape. Thus, a shape consistent constraint is needed to reduce the spatial distortion.

We suggest using a 3D segmentor to preserve shape consistency. The segmentor maps $x_i \rightarrow Y$, where i is the domain A or B. To constrain the geometric invariance of the generated volume we optimize the Cross Entropy+Dice loss [14] of the generated domain and its labels:

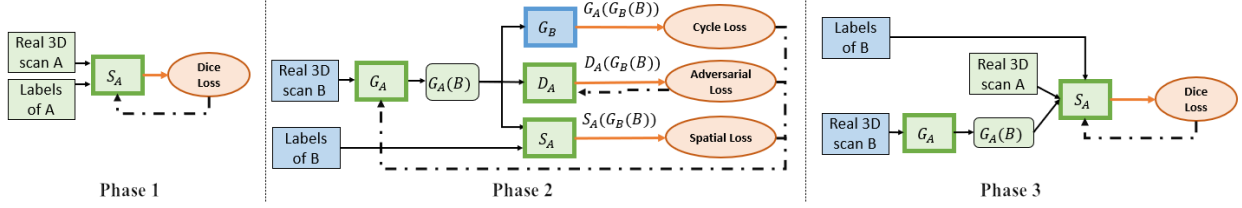$$\mathcal{L}_{spatial,A} = \mathcal{L}_{CE,A} + \mathcal{L}_{DICE,A}$$

Fig. 2. Overview of our domain adaptation and segmentation architecture. The architecture above is duplicated to handle both domains, a duplication where "A" is CT and "B" is MRI and vise versa. The flow is based on three chronological phases as described in training strategies.

$$\mathcal{L}_{DICE,A} = -\frac{2}{|K|} \sum_{k \in K} \frac{\sum_{i \in I} u_i^k v_i^k}{\sum_{i \in I} u_i^k + \sum_{i \in I} v_i^k}$$

where u is the softmax output of the network and v is a one hot encoding of the ground-truth segmentation y_A of the volume x_A. The generator's total loss function is composed of all the above constraints:

$$\mathcal{L}_A = \lambda_{adv}\mathcal{L}_{adv,A} + \lambda_{cycle}\mathcal{L}_{cycle,A} + \lambda_{spatial}\mathcal{L}_{spatial,A}$$

where λ_i is a trade-off parameter.

3.3. Segmentation

The segmentation network in our solution is based on a 3D U-net architecture [3]. In our architecture, there are two identical segmentors, one for each domain. Although each segmentor has its own source domain, both CT and MRI segmentors have the same target domain - cardiac segmentation labels. Thus, the segmentation task can be implemented on the original volume or on a generated synthetic volume, in both cases the ground-truth labels are identical. Formally, given input voxel X_A from domain A and its labels map Y_A, we define the following.

$$\mathcal{S}_A(X_A) = S_B(G_B(X_A)) = Y_A$$

Using this approach, we can train the segmentor with either real and synthesised data, it is important since segmentation networks usually require a lot of data to be trained on. Hence, the losses of the segmentors are defined by L_{seg} and $L_{seg,syn}$. Both are Cross Entropy+Dice losses, as used in *Fabian Isensee et al.*.

$$\mathcal{L}_{seg}(X_A, Y_A, S_A) = \mathcal{L}_{spatial}(Y_A, S_A)$$

$$\mathcal{L}_{seg,syn}(X_A, Y_A, S_B) = \mathcal{L}_{spatial}(Y_A, S_B(G_B(X_A)))$$

For each voxel of the input, the segmentor evaluates a vector of probabilities - one for each label. $S_A(X_A)_{i,Y_i}$ denotes the output of $S_A(X_A)$ on voxel i regarding to the probability of the ground-truth label of this voxel. $argmax(S_A(X_A)_i)$ will provide the label prediction of voxel i.

3.4. Training Strategies

Training the network consists of three phases, as we observed pre-training and fine-tuning the segmentor and generator results in better performances.

First, the segmentor is pre-trained for 100 epochs using only the original data. Then the generator and discriminator are trained leaning on the pre-trained segmentor from phase 1. The goal of this phase is to train a generator that can generate synthesized data in addition to the preprocessed synthesized volumes. The generator and discriminator are trained for 50 epochs without the spatial loss, and then for another 150 epochs with the spatial loss enforcing shape consistency. Last, after having a trained shape consistent generator, we train the segmentation network using the augmented and synthesised 3D volumes for 100 epochs.

3.5. Network Configurations and Implementations

Our network consists of segmentor, generator and discriminator modules for each domain.

The segmentation network is a 3D U-net consisted of 4 downsampling convolutions (maximum downsample rate is 16) and 4 upsampling using nearest interpolation, with convolutions of 3x3x3 kernel and stride 1.

The discriminators follow PatchGAN configurations [15], consists of 3 convolutional layers with kernels 4x4x4 and stride 2, and 2 convolutional layers with stride 1. For the first 4 layers, each convolutional layer is followed by a normalization layer and leaky ReLU with 0.2 slope parameter.

The generator is based on CycleGAN's U-net, adjusted to 3D volumes, using a skip-connection U-net, as it achieves faster convergence and locally smooth results [6]. We apply 5 downsampling with 3x3x3 kernel and stride 2, and upsample using nearest interpolation with 3x3x3 kernel and stride 1. We implemented our framework in PyTorch, and the training was done on 8 NVIDIA Quadro RTX 8000 GPUs. All the networks were optimized using the Adam optimizer with a learning rate of 2×10^{-4}.

Table 1. Segmentation performance comparison. The fifth and sixth rows show the boosted results by using shape consistent synthetic data, comparing SynSeg-Net, AdaOutput, PnP-AdaNet, SIFA and our method (using 4 labels and 7 labels), respectively.

Model	CT	MRI
SynSeg-Net	49.7	58.2
AdaOutput	51.9	59.9
PnP-AdaNet	54.3	63.9
SIFA	63.4	74.1
Ours - 4 labels	**88.2**	81.2
Ours - 7 labels	85.0	**81.8**

Table 2. Ablation study on our suggested net evaluating F1 score. The "Mode" column states the switched **off** component.

Mode	CT	MRI
Preprocessed Synthesized Volumes	58.7	61.7
Cross-Domain Synthesized Volumes	81.0	**81.9**
Shape Consistency	86.2	80.5
Full method	**88.2**	81.2

4. RESULTS

We use the Multi-Modality Whole Heart Segmentation (MMWHS) Challenge 2017 dataset for cardiac segmentation [16, 17]. This dataset consists of unpaired 20 CT and 20 MRI volumes with 7 segmented labels. We divided the dataset as commonly used to 80% training data and 20% test data. As *Cheng Chen et al.* is a major leading paper in this field and particularly on this dataset, we aligned our test and train samples to it and followed its test protocol for a better comparison. To evaluate the performance of the network segmentation accuracy we employ the commonly-used Dice similarity coefficient. As in previous works, the score is an unweighted average of the labels dice score, where each label's dice score is calculated separately. We compare our method with the SOTA unsupervised domain adaptation methods which utilize either feature alignment, image alignment, or their mixtures as shown in table 1. As part of our method we generated total of 400 3D augmented scans, other methods provided with a total of 21,600 2D augmented slices prepossessed as in [5]. Although the original dataset contains 7 labels for each volume, earlier works aimed to segment only 4 labels: ascending aorta (AA), left atrium blood cavity (LAC), left ventricle blood cavity (LVC), and myocardium of the left ventricle (MYO). Thus, we first trained our network to segment only those 4 labels and compared the results to previous unsupervised networks. All four previous compared models are using 2D slices for the segmentation and as can be seen in table 1, SIFA achieved on this dataset 63.4% CT and 74.1% MRI dice score. Our method which is the only method in table 1 that uses a 3D segmentor achieves 88.2% CT and 81.2% MRI dice score. This shows empirically that using 3D convolutions has an implicit effect of smoothness and z-coherency between the different slices.

As a second step, we aimed to segment all 7 labels and test the results compared to the 4 labels segmentation of our network. In addition to the first 4 labels, we also segmented: right atrium blood cavity (RAC), right ventricle blood cavity (RVC), pulmonary artery (PA). Our method achieves 85.0% CT and 81.8% MRI dice score. CT dice score is slightly decreased compared to 4 labels segmentation(3.6%). The MRI dice score slightly increased. The task of segmenting all 7 labels is more valuable since segmenting only 4 labels is not practical for real-life applications. Thus, our method shows promising results in segmenting multiple labeled volumes.

To observe the effectiveness of our suggested architecture we conducted ablation experiments as shown in table 2. First, we trained the network on the original dataset without preprocessed augmentations, the score of both CT and MRI are very low compared to the full method. This is expected since the original dataset is extremely small, but it also proves the effectiveness and importance of our augmentations. Another ablation study is to completely leave out the synthesized data and train the segmentor using only the preprocessed data. It stands out that there is a major difference between CT and MRI results in this case, While the CT domain performed a 7.2% improvement when used the synthesised data, the MRI domain shows the best result without any generated data at all. A possible explanation is that the MRI scans in this dataset are more diverse than the CT scans. Where in the MRI domain some scans are originally oriented to (P,S,R) and other scans to (L,S,P) and the size differs between scans, the CT scans are homogeneous in terms of orientation and size. We aim to better understand how to generate MRI synthesized scans in future studies. In the last ablation study, we did not use any shape consistency loss, which means we generated data without any segmentation information. It can be seen that the shape consistency constraint improves the score in both domains.

5. CONCLUSION

We have presented a method for Whole Heart Segmentation from a limited dataset using augmentations and generated shape consistent synthetic data. Our results on the MICCAI 2017 Multi-Modality Whole Heart Segmentation challenge show excellent performance for CT scans. As can be observed, using 3D segmentation rather than 2D segmentation on each Z-axis slice, achieve boosted results on both modalities. This is empirical proof of the added z-axis shape data.

6. COMPLIANCE WITH ETHICAL STANDARDS

7. ACKNOWLEDGMENTS

8. REFERENCES

[1] Chen Chen, Chen Qin, Huaqi Qiu, Giacomo Tarroni, Jinming Duan, Wenjia Bai, and Daniel Rueckert, "Deep learning for cardiac image segmentation: A review," *Frontiers in Cardiovascular Medicine*, vol. 7, pp. 25, 2020.

[2] Yundong Zhang, Huiye Liu, and Qiang Hu, "Transfuse: Fusing transformers and cnns for medical image segmentation," 2021.

[3] Özgün Çiçek, Ahmed Abdulkadir, Soeren S. Lienkamp, Thomas Brox, and Olaf Ronneberger, "3d u-net: Learning dense volumetric segmentation from sparse annotation," in *Medical Image Computing and Computer-Assisted Intervention – MICCAI 2016*, Sebastien Ourselin, Leo Joskowicz, Mert R. Sabuncu, Gozde Unal, and William Wells, Eds., Cham, 2016, pp. 424–432, Springer International Publishing.

[4] Fernando Pérez-García, Rachel Sparks, and Sébastien Ourselin, "Torchio: A python library for efficient loading, preprocessing, augmentation and patch-based sampling of medical images in deep learning," *Computer Methods and Programs in Biomedicine*, vol. 208, pp. 106236, Sep 2021.

[5] Cheng Chen, Qi Dou, Hao Chen, Jing Qin, and Pheng Ann Heng, "Unsupervised bidirectional cross-modality adaptation via deeply synergistic image and feature alignment for medical image segmentation," 2020.

[6] Zizhao Zhang, Lin Yang, and Yefeng Zheng, "Translating and segmenting multimodal medical volumes with cycle- and shape-consistency generative adversarial network," 2019.

[7] Raviteja Vemulapalli, Hien Van Nguyen, and Shaohua Kevin Zhou, "Unsupervised cross-modal synthesis of subject-specific scans," in *2015 IEEE International Conference on Computer Vision (ICCV)*, 2015, pp. 630–638.

[8] Ming-Yu Liu, Thomas Breuel, and Jan Kautz, "Unsupervised image-to-image translation networks," 2018.

[9] Konstantinos Kamnitsas, Christian Baumgartner, Christian Ledig, Virginia F. J. Newcombe, Joanna P. Simpson, Andrew D. Kane, David K. Menon, Aditya Nori, Antonio Criminisi, Daniel Rueckert, and Ben Glocker, "Unsupervised domain adaptation in brain lesion segmentation with adversarial networks," 2016.

[10] Phillip Isola, Jun-Yan Zhu, Tinghui Zhou, and Alexei A. Efros, "Image-to-image translation with conditional adversarial networks," 2018.

[11] Jun-Yan Zhu, Taesung Park, Phillip Isola, and Alexei A. Efros, "Unpaired image-to-image translation using cycle-consistent adversarial networks," 2020.

[12] David Abramian and Anders Eklund, "Generating fmri volumes from t1-weighted volumes using 3d cyclegan," 2019.

[13] Yongsheng Pan, Mingxia Liu, Chunfeng Lian, Tao Zhou, and Yong Xia, *Synthesizing Missing PET from MRI with Cycle-consistent Generative Adversarial Networks for Alzheimer's Disease Diagnosis: 21st International Conference, Granada, Spain, September 16-20, 2018, Proceedings, Part III*, pp. 455–463, 09 2018.

[14] Fabian Isensee, Jens Petersen, Andre Klein, David Zimmerer, Paul F. Jaeger, Simon Kohl, Jakob Wasserthal, Gregor Koehler, Tobias Norajitra, Sebastian Wirkert, and Klaus H. Maier-Hein, "nnu-net: Self-adapting framework for u-net-based medical image segmentation," 2018.

[15] Zhengxia Zou, Sen Lei, Tianyang Shi, Zhenwei Shi, and Jieping Ye, "Deep adversarial decomposition: A unified framework for separating superimposed images," in *2020 IEEE/CVF Conference on Computer Vision and Pattern Recognition (CVPR)*, 2020, pp. 12803–12813.

[16] Xiahai Zhuang and Juan Shen, "Multi-scale patch and multi-modality atlases for whole heart segmentation of mri," *Medical Image Analysis*, vol. 31, pp. 77–87, 2016.

[17] Xiahai Zhuang, "Challenges and methodologies of fully automatic whole heart segmentation: A review," *Journal of healthcare engineering*, vol. 4, pp. 371–408, 09 2013.